ACS OMEGA

Open Access

This article is licensed under CC-BY 4.0

http://pubs.acs.org/journal/acsodf

Article

A Theoretical Investigation of Nonadiabatic Dynamics and Time-Resolved NEXAFS Spectra of Uracil

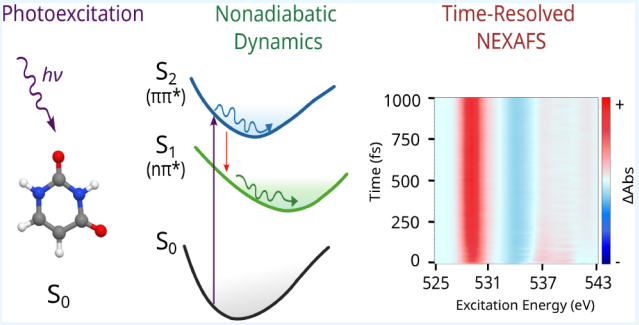
Bonasree Roy, Evgenii Titov, and Peter Saalfrank*

Cite This: *ACS Omega* 2026, 11, 56251−56264

Read Online

ACCESS | Metrics & More | Article Recommendations | Supporting Information

ABSTRACT: Uracil, a fundamental RNA nucleobase, exhibits complex excited-state dynamics governed by nonadiabatic processes that prevent photodamage. Upon photoexcitation, population initially reaches the bright $\pi\pi^*$ (S_2) state and subsequently relaxes to the dark $n\pi^*$ (S_1) state via conical intersections, before returning to the ground state on picosecond−nanosecond time scales. In this work, we investigate the ultrafast $S_2 \rightarrow S_1$ relaxation pathway using time-dependent density functional theory (TD-DFT)-based nonadiabatic surface hopping dynamics in combination with simulated time-resolved near-edge X-ray absorption fine structure (TR-NEXAFS) spectroscopy of oxygen, nitrogen and carbon K-edges. This combined approach allows us to capture both electronic and nuclear motion during the ultrafast relaxation and to identify atom-specific contributions to the decay process. In particular, $\pi\pi^*$ to $n\pi^*$ transitions occurring within the first 140 fs leave traces in O 1s and C 1s NEXAFS signals, indicating C═O bond elongations and torsional motion along the C═C bond, respectively. Overall, our results provide a detailed picture of population transfer, electronic-state trapping, and structural evolution in photoexcited uracil.



1. INTRODUCTION

The nucleobases have been the center of attraction for the study of molecular photodamage for several decades.[1−3] Although nucleobases are vulnerable to photodamage and subsequent mutations in the ultraviolet and even vacuum−ultraviolet region,[4−6] they rarely accumulate such damage. This is achieved by ultrafast relaxation to the ground state which provides the photostability to the molecules.[7−9] Among these nucleobases, uracil has served as a model system for understanding RNA photochemistry due to its relatively simple structure and well-characterized photophysics.

Previous literature has shown that uracil in the gas phase decays through two main channels. One is the dominant indirect pathway, where the population undergoes rapid $S_2(\pi\pi^*) \rightarrow S_1(n\pi^*)$ internal conversion and becomes transiently trapped in the S_1 state before returning to the triplet states and ultimately ground state on picosecond−nanosecond time scales. And another one, a minor, direct channel where it quickly depopulates the $\pi\pi^*$ state to reach the ground state within tens of fs.[10−13] In more detail, many (other) theoretical studies have shown that uracil undergoes ultrafast relaxation processes involving several conical intersections (CoIns) to populate the ground state, S_0, from the electronically excited states on ps or sub-ps time scales.[10,14−20] Quantum chemical calculations (such as TD-DFT, CASSCF, MRCIS and XMS-CASPT2) indicate that photoexcitation predominantly populates the bright S_2 state, characterized by a $\pi\pi^*$ configuration.[12] A few tenths of an electronvolt below S_2 is the dark S_1 state, which has predominantly $n\pi^*$ character. Nonradiative decay pathways are available through CoIns between S_2 and S_1, as well as between S_1 and S_0, facilitating efficient internal conversion. Alternatively, the population can remain trapped in the S_2 state for several picoseconds, before decaying either directly to the ground state or via the intermediate S_1 state.[13,14,18,21,22]

Ultrafast time-resolved spectroscopies have pointed out similar time scale for monoexponential decay to the ground state.[22,23] Also multiexponential decay has been established by ultrafast pump-probe photoionization experiments on isolated nucleic acid bases, with components in the femtosecond,[22,24] picosecond,[10,23] and nanosecond[25] ranges. Several authors have previously proposed that the shortest of these lifetimes, corresponds to decay from the initially excited state S_2, to the lower S_1 state.[15,16,24,26] The observed lifetimes can be significantly impacted by seemingly small changes of molecular structure. For instance, for thymine, which has a very similar structure to that of uracil only differing by one methyl group,

Received: June 15, 2026
Revised: September 1, 2026
Accepted: September 2, 2026
Published: September 8, 2026



© 2026 The Authors. Published by American Chemical Society

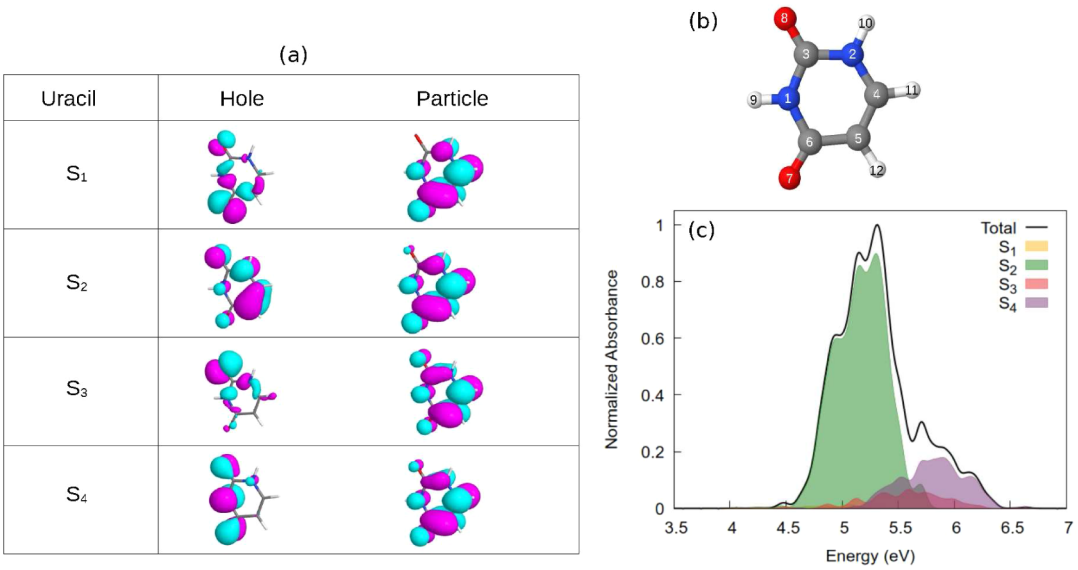


Figure 1. (a) Dominant NTOs for uracil, for S_1 to S_4. (b) Optimized geometry of uracil at the B3LYP+D3/def2-SVP+D3 level, with atom numbering indicated. (H: white, N: blue, O: red, C: grey.) (c) Absorption spectra (total and state-resolved) for 400 Wigner-sampled geometries for uracil at TD-B3LYP/def2-SVP level of theory, using eq 1 and S_1−S_4. Note that the S_1 signal (located between ∼4.0 and 5.5 eV) is weak.

the picosecond lifetime component differs by nearly three times, with 6.4 ps for thymine and 2.4 ps for uracil.[18,23]

One technique that has been used to probe nucleobases is X-ray absorption spectroscopy (XAS). XAS comprises a set of advanced techniques which allow for probing the local electronic structure of a molecule, with atomic resolution. Time-resolved X-ray absorption spectroscopy (TR-XAS) extends conventional XAS to the time domain by combining ultrafast pump−probe techniques with X-ray absorption measurements.[27,28] This made it possible to observe how molecules evolve after photoexcitation, revealing details of nuclear rearrangements[29] and electronic motion.[30] In parallel, theoretical studies use simulated spectra to interpret these processes and to examine the role of conical intersections in nonadiabatic dynamics,[31−33] by identifying changes in electronic-state populations,[20,34] analyzing nuclear motion,[20,35] and following wavepacket evolution.[36,37]

In this work, we focus on one specific type of XAS: Near-Edge X-ray Absorption Fine Structure (NEXAFS) spectroscopy, and its time-resolved variant, TR-NEXAFS. NEXAFS targets the near-edge region of an absorption spectrum,[37,38] complementing other techniques such as time-resolved photoelectron spectroscopy.[10] NEXAFS is particularly sensitive to local electronic structure, bonding environments, and unoccupied molecular orbitals. This makes it a powerful probe of ultrafast electronic and structural dynamics not only but in particular, for light elements such as C, N, and O, which are the key components of nucleobases. However, the interpretation of such spectra remains challenging without a direct link to the underlying nuclear and electronic dynamics. Here, we provide a direct correlation between non-adiabatic, Trajectory Surface Hopping (TSH) dynamics staying in the context of the mentioned indirect pathway (i.e., relatively long trapping in the S_1 state) and TR-NEXAFS spectra calculated "on the fly" using a previously developed Density Functional Theory Transition Potential Δ-Kohn-Sham (TP-DFT/ΔKS) approach[39,40] for the uracil molecule. In fact, it is the transient trapping in S_1 after excitation to S_2, *i.e.*, the decisive step in the dominant, indirect relaxation pathway, which is the focus of the present work (see below). By combining the two theoretical approaches just mentioned, we provide a detailed atom- and site-specific, and time-resolved analysis of the early excited-state dynamics of uracil using TR-NEXAFS at the O, N, and C K-edges. Our study treats *all* nuclear degrees of freedom (albeit classically), thus complementing a recent two-dimensional quantum dynamics work by Bäuml *et al.*[20]

Our paper is organized as follows. In the next chapter, Section 2, we describe computational methods and numerical details used in this work. In Chapter 2.4, we characterize (optical absorption) spectra as well as details of the non-adiabatic dynamics in uracil after initial photoexcitation, the latter based on TSH simulations. In Section 3.2, NEXAFS and TR-NEXAFS spectra at the O, N, and C K-edges are presented, which serve mostly as predictions for time-resolved experiments to come, and to demonstrate how electronic and nuclear motion translates into spectroscopic signals. A final Chapter 4 summarizes and concludes this work.

2. COMPUTATIONAL METHODS AND DETAILS

2.1. Ground-State Geometry and Vibrations

First, a ground-state (S_0) geometry optimization and vibrational frequency calculations by Normal Mode Analysis (NMA) were performed using Density Functional Theory (DFT) at the B3LYP/def2-SVP[41−43] level of theory. To improve the treatment of noncovalent interactions, Grimme's D3 dispersion correction with Becke-Johnson damping was employed,[44,45] as implemented in the ORCA 5.0.4 software package.[46] The optimized structure is shown in Figure 1b, along with atom numbering used later in this work. The vibrations are needed for Wigner sampling of initial geometries for dynamics and UV/vis spectra (see below).

2.2. Excited States and UV/Vis Absorption Spectrum

First, vertical excitation energies and oscillator strengths for the lowest few singlet excited states were computed, out of the optimized ground-state geometry, using linear-response time-dependent DFT (TD-DFT) at TD-B3LYP/def2-SVP level of theory. These properties were used both to guide the selection of bright initial states for dynamics, and to compute absorption spectra.

An UV/vis absorption spectrum of uracil was simulated to select the photoexcitation window used in dynamics. For this, 400 initial

https://doi.org/10.1021/acsomega.6c06959
ACS Omega 2026, 11, 56251−56264

conditions/geometries were generated using a Wigner distribution[47] based on the harmonic frequencies obtained from the NMA of the optimized ground state. For each of the initial conditions, the lowest four singlet states (S_1−S_4) were calculated at the TD-B3LYP/def2-SVP level, and used to determine an (approximate) UV/vis absorption spectrum, as

$$I(E) = K \sum_{i,\alpha} f_{i,\alpha} \exp\left[-\frac{1}{2\kappa^2}(E - E_{i,\alpha})^2\right] \quad (1)$$

Here, $E = \hbar\omega$ denotes the photon energy, $E_{i,\alpha}$ and $f_{i,\alpha}$ correspond to the calculated excitation energy and oscillator strength, respectively, for the $S_0 \rightarrow S_i$ transition of geometry ("snapshot") α (i = 1−4, α = 1−400). A Gaussian broadening to the individual transitions was used, with a broadening parameter, κ = 0.1 eV, as a default provided in the SHARC interface[48,49] (with which the dynamics were done). Further, K was chosen to normalize the maximal intensity of the broadened spectrum to 1.

2.3. Nonadiabatic Trajectory Surface Hopping Dynamics

To investigate the excited-state relaxation dynamics of uracil, nonadiabatic molecular dynamics simulations were performed using Tully's Fewest Switches Surface Hopping (FSSH) algorithm[50] as implemented in SHARC 3.0.[48,49] The quantum chemical backend used throughout the simulations was ORCA 5.0.4, employing the TD-B3LYP/def2-SVP level of theory with tight self-consistent field convergence criteria (as defined in ORCA). As for spectra, the five lowest singlet states (S_0−S_4) were included in the simulations. We note that triplet states were not considered in this work. As initial states for dynamics, those excited states, sampled at the geometries corresponding to the Wigner distribution, which had the highest transition dipole moments within an energy window from 4.0−6.0 eV, were selected. The chosen energy window covers the calculated absorption band of uracil (see Figure 1c). A total of 295 initial conditions were selected in this way, most starting in S_2, which is the first bright ($\pi\pi^*$) state.

The selected initial configurations were propagated for 1 ps with a nuclear integration time step of 0.5 fs. The nuclear motion was propagated using a velocity Verlet integration,[51] with 25 electronic substeps per nuclear time step to propagate the electronic wavefunction using a local diabatization scheme to facilitate efficient evaluation of nonadiabatic couplings.[52,53] Upon successful hops between electronic states, nuclear velocities were uniformly rescaled to conserve total energy. The hops were treated with standard hopping probabilities from SHARC. Additionally, an energy-based decoherence correction was included following the approach of Granucci and Persico.[54,55]

Of the initial set of 295 trajectories, 137 were retained for ensemble analysis. Trajectories that violated energy conservation (20 trajectories) exhibited excessively large energy differences in total energy between two consecutive time steps (>0.15 eV, 50 trajectories), showed nonphysical hopping energies (where after a successful hop, the energy changed by more than 1 eV, 35 trajectories) and trajectories that crashed due to convergence problems were discarded (53 trajectories). Analyzed properties are time-resolved state populations, state energies, geometric variables, and, most importantly, NEXAFS spectra.

2.4. (Time-Resolved) Near Edge X-ray Absorption Spectra

NEXAFS as well as TR-NEXAFS spectra were simulated, the latter to track the electronic and structural post-excitation evolution of uracil. The method to compute TR-NEXAFS spectra relies on computing pump-probe NEXAFS (PP-NEXAFS) spectra, where a valence excitation (pump) creates an excited state S_n (n > 0), which is then followed by an X-ray probe leading to site-specific core excitations into an unoccupied orbital. All virtual orbitals are used as final states. The spectra were calculated using the Density Functional Theory Transition Potential ΔKohn-Sham (TP-DFT/ΔKS) approach,[39,40] wherein a core spin-orbital ψ_i is populated with half an electron (as opposed to one electron) to approximate transitions to final, core-excited states efficiently (this approximation is also called the half-core-hole approximation). Absorption intensities were computed using Fermi's Golden Rule. Within the method, a ground state NEXAFS spectrum (at t = 0) is calculated as[39,40]

$$\sigma_{GS}(\omega, t = 0) = C\omega \sum_i \sum_f |\vec{e}\langle\psi_i|\vec{r}|\psi_f\rangle|^2 \delta(\varepsilon_f - \varepsilon_i - \hbar\omega) \quad (2)$$

Here, $\vec{e}$ is the field-polarization vector (averaging over possible polarization directions was done as described in ref 56), C a constant. Further, ψ_i is the (half-occupied) initial, KS core orbital i, ψ_f is a final (empty, but bound) orbital, and the $\varepsilon_{i,f}$ are corresponding energies. Orbitals and energies are obtained from self-consistent TP-DFT. Within TP-DFT/ΔKS, in addition the lowest excitation energy is shifted to align with the energy difference between the first fully core-excited state and the ground state, obtained from a separate ΔKS calculation. Note that initial-state/atom resolved cross sections, $\sigma_{GS,i}$, can simply be obtained by selecting a certain initial orbital/atom, without summing over i. The same way, one can calculate total pump-probe NEXAFS spectra, $\sigma_{PP}(\omega, t)$, where (the half-electron) core excitation starts from a valence-excited reference state, S_n (n > 0). Again, a ΔKS shift is applied, but now to align with the energy difference between valence-excited and core-excited states (see refs [39,40] for details). The PP-NEXAFS spectrum $\sigma_{PP}(\omega, t)$, and initial-state/atom resolved variants of it, $\sigma_{PP,i}(\omega, t)$, are here time-dependent, since they arise from a TSH scheme, *i.e.*, the atoms move. This way, TR-NEXAFS spectra are generated "on the fly".

In practice, we combine TSH with the PSIXAS plugin,[40] interfaced with the Psi4 electronic structure package.[57] The B3LYP/def2-SVP level of theory (*i.e.*, the same as for the TSH calculations) was employed for all X-ray absorption simulations. For each selected trajectory, (PP-)NEXAFS spectra were computed at regular 10 fs intervals from 0 to 1000 fs. Each spectrum was constructed by identifying, from the SHARC/ORCA outputs at time t, the trajectory's current active state, S_n, and geometry, and the corresponding (PP-)NEXAFS spectrum is calculated. Shown below are *difference spectra* (which are usually reported in experimental studies), computed as

$$\Delta\sigma(\omega, t) = \langle\sigma(\omega, t)\rangle - \langle\sigma_{GS}(\omega, t = 0)\rangle \quad (3)$$

Here, $\langle\sigma(\omega, t)\rangle$ is an *ensemble-averaged* (PP-)NEXAFS spectrum at time t, calculated as PP-NEXAFS spectrum if the system is in an excited state S_n (n > 0) at time t, or as a ground state NEXAFS spectrum when the system is in S_0 at that time. Further, $\langle\sigma_{GS}(\omega, t = 0)\rangle$ denotes the *ensemble-averaged* GS-NEXAFS spectrum, at t = 0. Again, both total and atom/site-resolved spectra can be calculated. Below, the TR-NEXAFS spectra for oxygen, nitrogen, and carbon K-edges were calculated to monitor atom-type and even site-specific changes. A subset of the SHARC trajectories was selected for the TR-NEXAFS analysis. Since the focus of the present work is the early $S_2 \rightarrow S_1$ internal conversion, mainly trajectories initiated in the S_2 state were considered, resulting in an ensemble of 120 trajectories for the O 1s and N 1s simulations. For the C 1s calculations, the ensemble was further reduced to 56 trajectories because the larger number of inequivalent carbon atoms substantially increased the computational cost and memory requirements.

All NEXAFS spectra were broadened using a Gaussian function with κ = 1.8 eV instead of the delta function in eq 2. The broadening parameter has been previously established in a separate, yet unpublished experimental-theoretical collaborative *gas-phase* TR-NEXAFS study. The same broadening was also used in an earlier theoretical TR-NEXAFS investigation.[58]

3. RESULTS AND DISCUSSION

3.1. Electronic Excitations, Post-Excitation Dynamics

3.1.1. Vertical Excitation Energies and Nature of Excited States. First, vertical excitation energies of uracil out of the ground state were computed using (TD-B3LYP/def2-SVP) at the B3LYP/def2-SVP+D3 geometry. Table 1 lists the first ten singlet excited states, showing their excitation energies,

https://doi.org/10.1021/acsomega.6c06959
ACS Omega 2026, 11, 56251−56264

Table 1. Vertical Excitation Energies and Oscillator Strengths for Uracil Computed Using TD-B3LYP/def2-SVP

Transition	E_i (eV)	Oscillator Strength, f_i
$S_0 \rightarrow S_1$	4.680	0.000
$S_0 \rightarrow S_2$	5.322	0.124
$S_0 \rightarrow S_3$	5.818	0.000
$S_0 \rightarrow S_4$	5.996	0.037
$S_0 \rightarrow S_5$	6.251	0.000
$S_0 \rightarrow S_6$	6.659	0.000
$S_0 \rightarrow S_7$	6.727	0.107
$S_0 \rightarrow S_8$	6.785	0.000
$S_0 \rightarrow S_9$	7.363	0.013
$S_0 \rightarrow S_{10}$	7.740	0.429

E_i, and corresponding oscillator strengths, f_i. The S_2 state exhibits the highest oscillator strength (0.124), of states below 6 eV, identifying it as the most optically accessible transition from the ground state in this energy range. It lies at 5.32 eV, followed by S_4 at 5.99 eV, which also has a moderate oscillator strength (0.037). The state energies of S_1 to S_4 are in excellent agreement with earlier TD-B3LYP/6-31G* calculations.[59] In that reference, also better basis sets (and other methods) were tested, shifting excitation energies somewhat: At TD-B3LYP/aug-cc-pVTZ level, for example, the energies of S_1, S_2, S_3 and S_4, are 4.64, 5.11, 5.64, and 5.74 eV, respectively, *i.e.*, red-shifted by up to ∼0.2 eV w.r.t. Table 1. Experimentally, the lowest bright state, S_2, is at 5.08 eV (in solution) according to ref 60.

The electronic characters of low-lying excited states S_1−S_4 were characterized via natural transition orbital (NTO)[61] analysis. In Figure 1a, the dominating NTO "hole" and "particle" pairs are shown, for the lowest four vertical excitations. The first excited state (S_1) predominantly exhibits $n\pi^*$ character, originating from nonbonding lone pairs on oxygen atoms transitioning to an antibonding π^* orbital. The bright S_2 state is of $\pi\pi^*$ character, involving transitions between a delocalized bonding π-orbital and an antibonding π^* orbital. The third excited state (S_3) is of $n\pi^*$ character again and optically dark. The next bright state, S_4, is of $\pi\pi^*$ type and bright. The shape of the hole NTOs of S_1 and S_2 are similar to the highest n (HOMO−1) and π (HOMO) KS orbitals (see ref 59, for example), and the shape of all particle NTOs shown, is similar to the π^* (LUMO) orbital.

We also compared the TDDFT-B3LYP vertical excitation energies with previous experimental data and higher-level theoretical values.[9,12,62] The calculated excitation energies (4.68, 5.32, and 5.82 eV) are in good agreement with the available low-lying experimental values of 4.38, 5.1, and 6.0 eV for S_1−S_3 states, respectively.[9,12] The calculated TDDFT values also compare favorably well with the CASPT2 results, which predicts S_1 to S_3 energies in the range of 4.9−6.41 eV and 4.85−6.02 eV depending on the chosen active space, while CASSCF predicts the excitation values in the range of 5.13−7.07 eV and 4.83−7.33 eV (a bit higher, as it lacks the dynamic correlation) depending on the chosen active space.[9] We note, however, that the S_3 character is highly sensitive to the chosen active space in case of CASSCF and CASPT2. EOM-CCSD yields somewhat higher excitation energies (5.17, 5.56, and 6.52 eV for S_1, S_2, and S_3, respectively).[62] Overall, the TDDFT/B3LYP excited states reproduce the relative ordering of the low-lying excited states (S_1 is $n\pi^*$, S_2 is $\pi\pi^*$) and TD-B3LYP excitation energies are in reasonable agreement with both experiment and higher-level correlated electronic structure methods in the Franck−Condon region, supporting its suitability as the starting point for the present nonadiabatic dynamics simulations.

The features of these electronic transitions are directly reflected in the simulated absorption spectrum for 400 sampled geometries (Figure 1c), which shows a dominant band around 5.3 eV attributed to excitation into S_2 (green). The second intense peak (less intense than S_2 though) corresponds to S_4, consistent with its moderate oscillator strength (violet). These features agree well with previous gas-phase absorption spectra of uracil.[9,13,15,59,62−64]

3.1.2. Post-Excitation Dynamics by Trajectory Surface Hopping. To simulate the ultrafast dynamics following photoexcitation, we initiated the 295 trajectories selected from the Wigner-sampling as described above, by including the S_1−S_4 excited states. In the TSH dynamics, done by SHARC, also the S_0 ground state was included. As said earlier, most trajectories started in state S_2, namely 234 (∼79.3%), while 14 (∼4.7%) started from S_3, and 47 (∼15.9%) from S_4. Out of these, 137 trajectories were retained after applying filters for energy conservation and unrealistic fragmentations (see the Methods section).

Figure 2a shows the evolution of electronic state populations over time. It is seen that the initially dominant S_2 population is

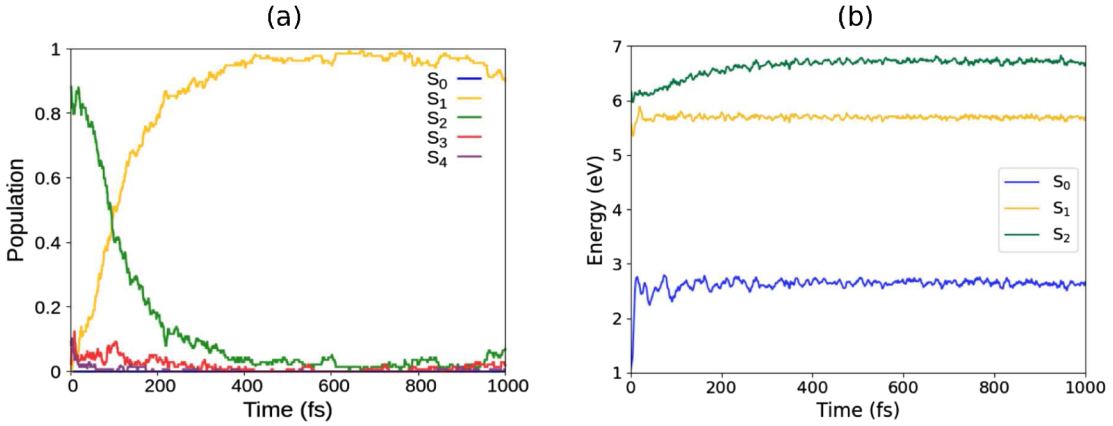


Figure 2. (a) Ensemble-averaged electronic state populations of states S_0−S_4 for the uracil molecule as a function of time. (b) Ensemble-averaged energies of states S_0−S_2 as a function of time.

https://doi.org/10.1021/acsomega.6c06959
ACS Omega 2026, 11, 56251−56264

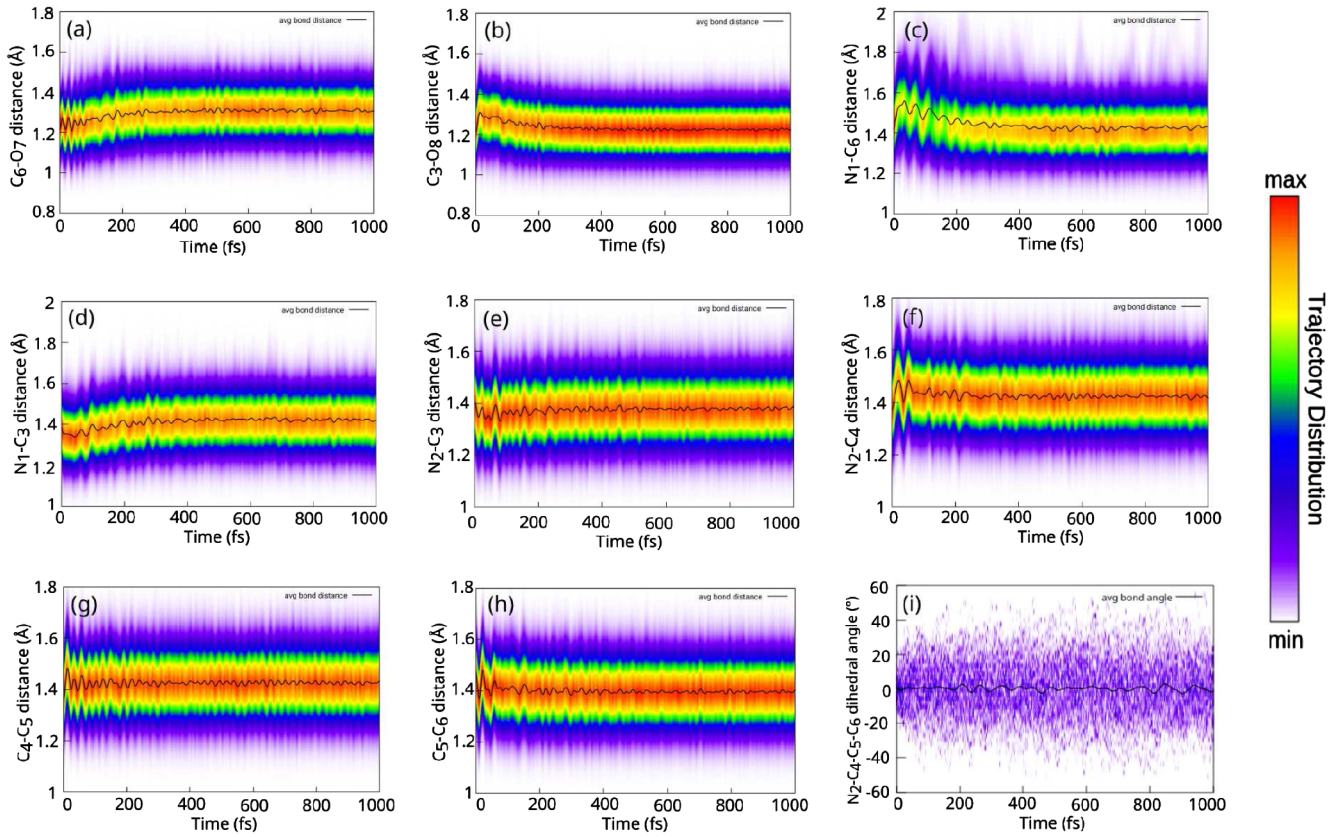


Figure 3. Ensemble-averaged bond lengths and angles in uracil after photoexcitation. (a) C6−O7 bond length; (b) C3−O8 bond length; (c) N1−C6 bond length; (d) N1−C3 bond length; (e) N2−C3 bond length; (f) N2−C4 bond length; (g) C4−C5 bond length; (h) C5−C6 bond length; (i) ensemble-averaged N2−C4−C5−C6 dihedral angle. The colored patterns give the probability distributions and the solid black lines are the averaged values over all analyzed trajectories. Atom numbering is according to Figure 1b.

quickly transferred to the first excited state, S_1. Fitting the rise in S_1 ($n\pi^*$) population to a single-exponential function ($1 - \exp(-t/\tau)$), yields a characteristic time constant of approximately 140 fs. Mechanistically, after excitation to the bright $\pi\pi^*$ (S_2) state, the system undergoes rapid internal conversion to the dark $n\pi^*$ (S_1) state via a well-characterized S_2/S_1 conical intersection as mentioned earlier. We also note that for a larger ensemble of 186 trajectories (including all trajectories that reached 1 ps, some of which are not included in the 137-trajectory ensemble based on the energy-related criteria described in the last paragraph of Section 2.3), the S_1 time constant is very similar, 141 fs. Furthermore, for the smaller samples of 120 and 56 trajectories used for TR-NEXAFS calculations, the S_1 time constants are 144 and 127 fs, respectively.

No significant population transfer to S_0 is observed within our simulation window of 1 ps. The lack of ground-state recovery, together with the low populations in S_3 and S_4 (see below), suggest that the system becomes transiently trapped on the S_1 surface. The absence of ground state (S_0) relaxation can partly be explained by the electronic structure of uracil, where the S_1 state is known to host a local minimum that is only weakly coupled to the S_1/S_0 conical intersection, thus functioning as a transient energy trap.[9,12] The trapping of S_1 is also consistent with a persistent energetic gap between the S_1 and S_0 surfaces according to our simulations (*cf.* Figure 2b), which prevents relaxation to the ground state. We note that the potential energies shown in Figure 2b represent the dynamical evolution rather than potential energy scans.

We note that the S_1 trapping found here could also have methodological causes (TD-DFT underestimates $S_1 \rightarrow S_0$ transitions, we have not included spin-orbit coupling to triplet states, and the propagation time is comparatively short). Furthermore, the absence of $S_1 \rightarrow S_0$ hops is also likely influenced by the use of TD-DFT, a single-reference method that is generally less reliable in accurately describing regions near conical intersections, notably those involving S_0. We also note that no S_0/S_1 energy gap criterion was used in our simulations to enforce transitions to S_0. Also, the inclusion of triplet state is expected to lead to S_1 depopulation via intersystem crossing,[10] thus reducing the trapping effect. On the experimental side, it has been shown that uracil and related molecules can exhibit delayed fluorescence (or phosphorescence), indicating that the lowest $n\pi^*$ state is indeed transiently trapped.[14,65] Further, Ghafur *et al.*[21] reported biexponential decay dynamics with a fast sub-100 fs component followed by a much slower relaxation to S_0 on the picosecond time scale of around 3 ps. Recently, Faccialà *et al.*[10] reported ultrafast $S_2 \rightarrow S_1$ internal conversion within 17 ± 4 fs and showed that the deactivation pathway moves through an intersystem crossing, with $S_1 \rightarrow T_1/T_2$ conversion taking place in 1.6 ± 0.4 ps. They also reported on a minor pathway proceeding via ultrafast (tens of fs) $\pi\pi^* \rightarrow S_0$ internal conversion. On the theory side, some studies have reported $S_1 \rightarrow S_0$ internal conversion in uracil. But even there, in multireference simulations, only a small fraction of trajectories exhibited relaxation to the ground state.[12] Also Richter *et al.*[9] have shown that population can transfer from the S_1 ($^1n\pi^*$)

https://doi.org/10.1021/acsomega.6c06959
ACS Omega 2026, 11, 56251−56264

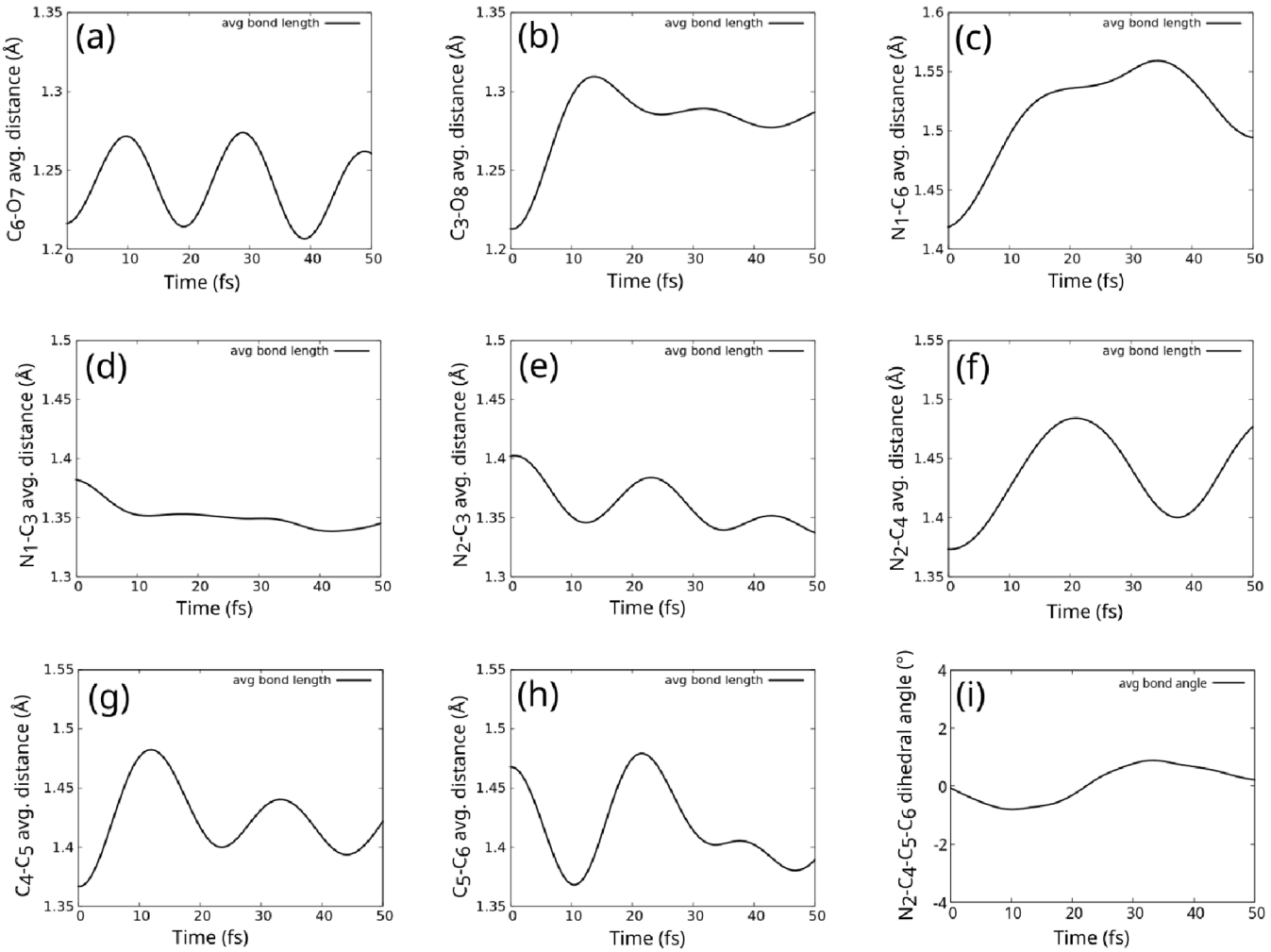


Figure 4. Averaged bond lengths and angles (averaged over all trajectories) in uracil after photoexcitation upto 50 fs. (a) C6−O7 bond length; (b) C3−O8 bond length; (c) N1−C6 bond length; (d) N1−C3 bond length; (e) N2−C3 bond length; (f) N2−C4 bond length; (g) C4−C5 bond length; (h) C5−C6 bond length; (i) ensemble-averaged N2−C4−C5−C6 dihedral angle. Atom numbering is according to Figure 1b.

state to the energetically accessible T_2 ($^3\pi\pi^*$) state, followed by rapid internal conversion to T_1 before returning to S_0 with decay time of 2−3 ps. Semiempirical surface hopping simulations suggest that ground-state recovery is delayed, with approximately 90% of the population returning to S_0 only after about 1.3 ps,[64] *i.e.*, on somewhat longer time scales. Consequently, while the present simulations only emphasize the indirect but dominant, relaxation channel, they remain consistent with experimental evidence for transient population trapping in the $n\pi^*$ state and provide insight into the spectroscopic signatures associated with this pathway (presented in Section 3.2). Since our focus here is on this indirect relaxation pathway involving transient population of the lowest $n\pi^*$ state, the use of TD-DFT is justified.

In Figure 2a, also populations of states S_3 and S_4 are shown, which were selected with small probability as initial states (see above). As a consequence, we note that both S_3 and S_4 exhibit only transient population following excitation. A small rise in population of S_3 is observed within the first 50−100 fs due to nonadiabatic transitions from state S_4 to S_3. However, this population increase is short-lived, and both states quickly depopulate, predominantly funneling into S_1 (*i.e.*, $S_3 \rightarrow S_2 \rightarrow S_1$). This is consistent with the expected ultrafast internal conversion dynamics in pyrimidine bases, where the excited-state manifold is densely packed and internal conversion is efficient.[9,12,14,15]

3.1.3. Geometrical Changes during Nonadiabatic Transitions. To elucidate the structural response of uracil following photoexcitation, we examined key geometrical parameters during the early stages of nonadiabatic dynamics. In particular, we focused on changes in carbonyl and ring-associated bond lengths to assess how nuclear motion contributes to internal conversion.

Figure 3a and b show the time evolution of the C6−O7 and C3−O8 carbonyl bond lengths for the 1 ps simulation interval, with atom numbering given in Figure 1b. Both bond lengths oscillate on the time scale of CO vibrations (of ∼20 fs for a vibration with ∼1700 cm^{-1}, see also Figure 4). Then they gradually elongate (C6−O7) or shorten (C3−O8), on the time scale of a few hundred fs, which is the time scale of the $S_2 \rightarrow S_1$ transition. This dynamic redistribution suggests a rapid modulation of electron density within the conjugated π-system, consistent with a transition between delocalized $\pi\pi^*$ and more localized $n\pi^*$ states. We also find substantial out-of-plane motion of the O7 atom, previously characterized in multi-reference studies as the defining feature of the out-of-plane-O intersection,[13] which is reflected in altered C−O bond geometries in our trajectories.

https://doi.org/10.1021/acsomega.6c06959
ACS Omega 2026, 11, 56251−56264

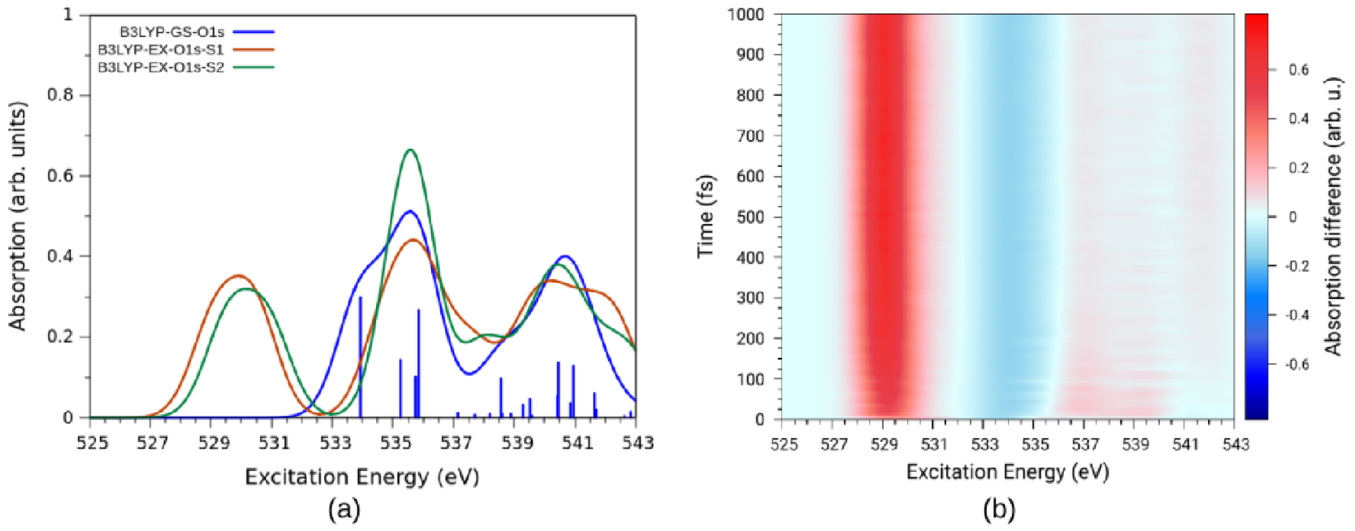


Figure 5. (a) Broadened O 1s GS-NEXAFS spectrum with underlying stick spectrum, both in blue, and PP-NEXAFS spectra for the S_1 (red) and S_2 states (green) of uracil. (b) Time-resolved O 1s NEXAFS spectrum (TR-NEXAFS) following photoexcitation.

Beyond the carbonyl groups, notable changes are observed in N1−C6 and N1−C3 bonds (Figure 3c,d). These changes are known to occur near S_2/S_1 hopping geometries,[12] and are structurally aligned with puckering and torsional displacements which drive access to conical intersections.[12,13] In contrast, the N2−C3 and N2−C4 bonds remain relatively unaffected over time, as shown in Figure 3e,f.

The C4−C5 double bond, part of the ethylenic moiety implicated in one known S_1/S_0 CoIn pathway,[9,12,15] exhibits pronounced damped oscillatory behavior during the first ∼140 fs (see Figure 3g).

In general, the observed geometrical changes are a result of electronic transitions and post-excitation nuclear motion. For instance, after sudden initial $S_0 \rightarrow S_2$ excitation, the ground-state C4−C5 bond length is too long in the excited state, because a π (C4−C5 bonding) → π^* (C4−C5 antibonding) transition took place, *cf.* Figure 1. The molecule starts to adapt to the new electronic structure, visible by an elongation of the C4−C5 bond length within the first 10 fs or so, corresponding to about half of the vibrational period of the C−C stretch mode (also ∼20 fs). Then it undergoes the mentioned, damped oscillation (black line in panel(g)), toward an averaged C4−C5 bond length of slightly above 1.4 Å, which is half-way between a C−C double (∼1.34 Å) and C−C single-bond length (∼1.54 Å). Similarly to C4−C5, also the C−O bond lengths C3−O8 and C6−O7 show a rapid expansion after initial $S_0 \rightarrow S_2$ excitation. This is in agreement with experimental findings based on O 1s X-ray photoelectron spectra in ref 10. While the C4−C5 bond length does not change a lot during the $S_2 \rightarrow S_1$ transitions around ∼140 fs, others, like the C3−O8 and C6−O7 bond lengths mentioned above show a clear overall trend during this transition. The precise nature of these trends, however, cannot be easily deduced from the shape of participating NTOs alone, in particular not from those evaluated at the ground state geometry given in Figure 1.

Overall, however, the structural dynamics observed in our TD-DFT based surface hopping simulations are consistent with motion toward well-characterized S_2/S_1 intersection seams involving puckering, bond elongation, and lone pair reorganization.[9,10,12,13,15,64] We note that our time scale for the $S_2 \rightarrow S_1$ transition ∼140 fs, is somewhat longer than the experimental one found in ref 10, of 17 ± 4 fs. Interestingly, the same 17 fs were inferred from EUV-TRPES experiments.[66] However, SCS-ADC(2) surface hopping simulations used in ref 10. yield a $\pi\pi^*$ decay time of ∼160 fs,[10,67] which is close to our TD-DFT result. We note though that the computational time scale of $S_2 \rightarrow S_1$ internal conversion is very sensitive to the electronic structure method used for nonadiabatic dynamics, with CASSCF predicting 575.5 fs and XMS-CASPT2 predicting only 12.5 fs.[12,68] Also, in our work we find no evidence for direct $\pi\pi^* \rightarrow S_0$ transitions, which was an observed minority channel according to ref 10. Despite the difference between the experimental and TD-DFT lifetimes, we expect the trends observed in the TR-NEXAFS spectra reported in the next section remain valid, as they track a transition between different electronic states, only with changes occurring faster in the experimental system.

3.2. Stationary and Time-Resolved NEXAFS Spectra

To directly correlate the ultrafast excited-state dynamics of uracil with time-resolved electronic and structural changes, we computed TR-NEXAFS spectra at the O 1s, N 1s, and C 1s edges. First, the stationary absorption characteristics of the ground state (GS), as well as idealized PP-NEXAFS spectra when S_1 or S_2 states are assumed to have been completely pre-excited initially (no admixture of the GS), all at the optimized GS geometry, are presented. Then TR-NEXAFS signals will be computed, using geometries and state populations from the TSH trajectories. All NEXAFS spectra were calculated using the TP-DFT/ΔKS approach as described earlier.

3.2.1. O 1s Stationary and TR-NEXAFS Spectra. Let us start with the stationary ground state (GS) O 1s NEXAFS spectrum. The broadened O 1s absorption spectrum in the ground state, shown as blue line in Figure 5a and denoted there as "B3LYP-GS-O1s", is characterized by the onset of intensity above ∼532 eV, with prominent features extending from 534−537 eV and from 539−543 eV. These transitions originate from excitations of the oxygen 1s core electron(s) into the lowest unoccupied orbitals of uracil. In uracil, there are two O atoms, O7 and O8, and the shoulder at 534 eV, is due to the excitation from the O7 1s orbital, to the lowest π^* orbital (the LUMO), while the intensity around the maximum

https://doi.org/10.1021/acsomega.6c06959
ACS Omega 2026, 11, 56251−56264

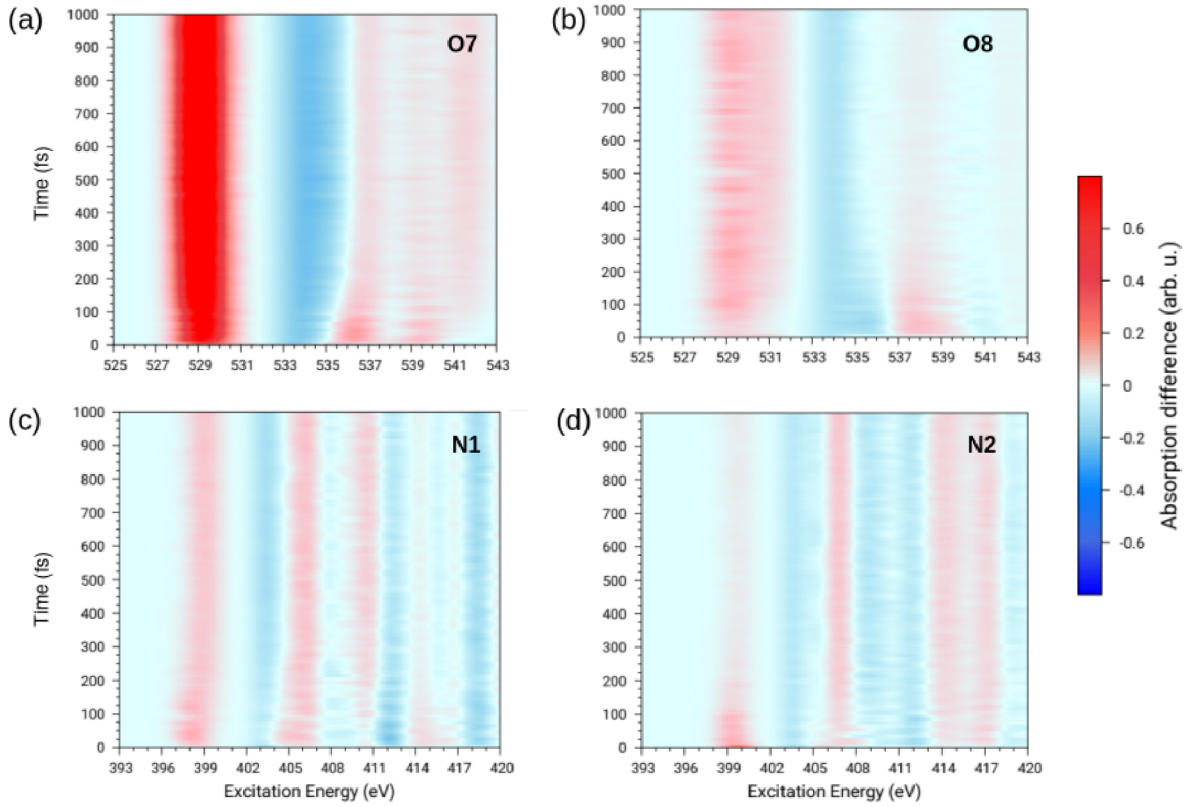


Figure 6. Atom-resolved TR-NEXAFS of the uracil molecule. (a) and (b) represent the O7 and O8 atom-resolved TR-NEXAFS, (c) and (d) represent the N1 and N2 atom-resolved TR-NEXAFS. See Figure 1b for atom numbering.

of the peak is dominated by the transition of O8 1s, to the same final orbital. More precisely, the two lowest-energy transitions in the O 1s absorption peak around 534−537 eV, are found at 533.9 eV (O7) and 535.2 eV (O8), and are shown (with intensities) as blue sticks underlying the broadened spectrum. (Note that also other transitions contribute to the main peak.) Experimentally, the gas phase GS O 1s NEXAFS spectrum of uracil was determined in ref 69. The spectrum has a similar overall shape as here, with a higher resolution than chosen here. In experiment, two lowest-energy peaks called "A" and "B" are found, at 531.4 and 532.4 eV, respectively. Obviously, our theoretical spectrum is blue-shifted by about 2−3 eV, and the peak splitting somewhat overestimated by 0.3 eV. Note that in ref 69, also theoretical O 1s GS NEXAFS spectra were determined, using the more accurate ADC(2)/6-31+G method. This method gives the lowest two peaks with the same assignment as here, appearing at 533.5 and 534.5 eV, respectively, after an overall, empirical shift of −2.15 eV was made. In our work, we do not make such empirical shifts, since we are mostly interested in changes of spectra during dynamics (see below).

Upon valence excitation, in the first excited state, S_1 ($n\pi^*$), an electron is promoted from a nonbonding n orbital, to the previously empty π^* orbital, giving rise to a modified NEXAFS spectrum. The n-orbital now being partially empty, allows O 1s → n transitions to happen, which leads to an intense lower-energy peak with maximum intensity at 529−530 eV in the PP-NEXAFS spectrum (red line in Figure 5a, labeled "B3LYP-EX-O1s-S1"). The higher-energy peak corresponding to the O 1s → π^* transitions is also affected, since π^* is now partially filled. Similarly, for the S_2 PP-NEXAFS spectrum (green line in Figure 5a, labeled "B3LYP-EX-O1s-S2"), the pre-excitation causes a $\pi \rightarrow \pi^*$ transition, leading to a hole in the π-orbital, which, upon probe excitation, causes another low-energy satellite at 530−531 eV in the NEXAFS spectrum due to O 1s → π^* transitions. To the best of our knowledge, no PP-NEXAFS spectra of gas-phase uracil have been measured so far.

These features are clearly reflected in the (atom- and trajectory-averaged) oxygen K-edge TR-NEXAFS difference spectrum (Figure 5b), calculated via eq 3. Recall that in the photodynamics, ∼79% of trajectories start in the S_2 state. As a consequence, we see a strong positive absorption band centered around 529 eV, corresponding to the lowest-energy feature in the PP-NEXAFS (S_2) spectrum in Figure 5a, green line. We also see a weaker, transient feature near 537 eV. At early times (0−20 fs), the 529 eV band appears sharp and intense, but it rapidly broadens and stabilizes by approximately 140 fs. This evolution reflects the effects of vibronic coupling and nuclear ensemble dispersion, as the molecule (trajectories) explore(s) a range of nuclear geometries on the excited-state potential energy surfaces. This behavior is in line with prior time-resolved XAS simulations, where the evolving spectral signatures were attributed to population-weighted contributions from the S_2 and S_1 states and their associated nuclear geometries.[20]

The higher-energy absorption feature initially centered around 536 eV (Figure 5b), displays a distinct temporal evolution that is highly diagnostic of excited-state relaxation pathways. At early times (within the first 20 fs), the absorption begins near 536 eV and progressively shifts toward higher energies, peaking around 537 eV before decaying in intensity after 100 fs. This gradual blue-shift indicates a dynamic change in the local electronic environment of the carbonyl oxygen

https://doi.org/10.1021/acsomega.6c06959
ACS Omega 2026, 11, 56251−56264

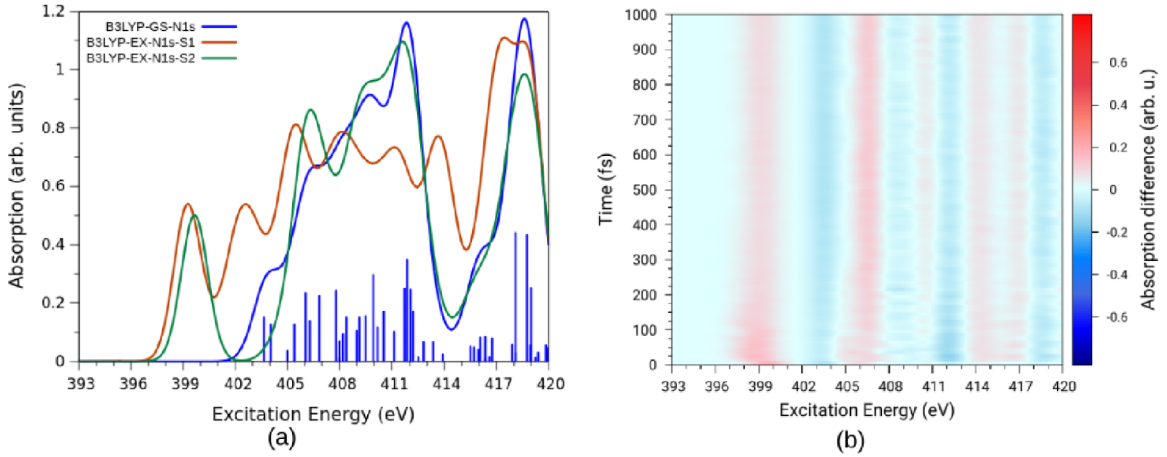


Figure 7. (a) Broadened N 1s GS-NEXAFS spectrum (with underlying stick spectrum) and PP-NEXAFS spectra for the S_1 and S_2 states of uracil. (b) Time-resolved N 1s NEXAFS spectrum (TR-NEXAFS) following photoexcitation.

atoms and is consistent with the onset of nonadiabatic transitions from the initially excited S_2 ($\pi\pi^*$) state to the lower-lying S_1 ($n\pi^*$) state. The precise nature of blue-shift and fading of this signal is difficult to analyze, due to the underlying nuclear dynamics. However, the intensity loss and blue-shift at longer times are already consistent with the lower intensity/blue-shift of this peak in the stationary PP-NEXAFS (S_1) spectrum, compared to the corresponding peak in the PP-NEXAFS (S_2) spectrum.

A prominent negative signal is also observed between 532−536 eV, most intense at 534 eV. This feature corresponds to a ground-state bleach after photoexcitation. At time zero, the bleach spans from 533−535 eV, but over the first 100−150 fs, it shifts toward 536 eV (its right side), forming a curved temporal profile before stabilizing.

We also performed an atom-resolved analysis of the O 1s TR-NEXAFS spectrum (Figure 6a,b). A pronounced asymmetry is observed between the two oxygen atoms, O_7 and O_8, reflecting their distinct electronic roles during the excited-state dynamics. O_7, bonded to C_6 exhibits dominant and dynamically evolving spectral features, while O_8, bonded to C_3 between the two nitrogen atoms (see Figure 1b), shows a relatively weaker response but also dynamically evolving.

The O7-resolved spectrum displays two key positive band features: a strong, stationary absorption near 529 eV and a dynamic peak that shifts from approximately 535 eV to 537 eV within the first ∼140 fs. A ground-state bleach is also present, initially peaking at 534 eV and shifting its right side to 536 eV in parallel with the 535 to 537 eV positive feature. This correlated blue-shift closely tracks the lengthening of the C6−O7 bond observed in the excited-state dynamics (Figure 3a). We note that here, and in what follows, we compare changes in *ensemble-averaged* TR-NEXAFS with evolution of *ensemble-averaged* geometrical parameters.

In contrast, for the O8-resolved spectrum, a weak and relatively stationary peak at 529 eV is concurrent with the shortening of the C3−O8 bond (Figure 3b) The next features of the O8 spectrum are the ground state bleach at around 534 eV and a positive band at 538 eV. The border between these features experiences a red-shift with time in around 150 fs, and the positive band also looses its intensity within this time. As a result, the O8 site contributes less to the evolving absorption spectrum, due to diminished oscillator strength of the S_1 excited state.

Overall, our O 1s NEXAFS spectra are associated with ultrafast $S_2 \rightarrow S_1$ internal conversion, consistent with the surface hopping results showing system relaxation within the 140 fs timeframe. The redistribution of valence electron density is directly reflected in the evolving spectral features of a nonadiabatic relaxation pathway from the more delocalized $\pi\pi^*$ excitation to the more localized $n\pi^*$ state in uracil.

3.2.2. N 1s Stationary and TR-NEXAFS Spectra. The calculated N 1s GS-NEXAFS and stationary S_1 and S_2 PP-NEXAFS spectra of uracil are shown in Figure 7a. For the GS spectrum, two main bands are observed in the energy range shown, a highly structured lower-energy one extending from ∼403−413 eV, and a higher one from ∼415 to above 420 eV. More precisely, the two lowest-energy transitions from N 1s to the LUMO (π^*), are at 403.7 eV for N1, and at 404.0 eV for N2, respectively, *i.e.*, both are under the shoulder around 404 eV in the figure (see also the underlying stick spectrum). Experimentally, this shoulder is a (better resolved) signal called "A" in ref 69, with its maximum at 401.4 eV. Calculations in ref 69 on the ADC(2)s/6-311+G* level show that the two lowest-energy N 1s NEXAFS signals dominate the "A" peak, and are found, after an empirical red-shift by −3.80 eV, at 400.5 eV (N1 1s → π^* (LUMO) transition) and 400.8 eV (N2 1s → π^* (LUMO) transition), respectively. Hence, our TP-DFT/ΔKS calculations are blue-shifted again by ∼2−3 eV w.r.t. experiment; the assignment and splitting of the two lowest peaks are consistent with the ADC calculations in ref 69.

According to Figure 7, for the PP-NEXAFS spectra strong new peaks are observed at 399 eV (S_1, red) and close to 400 eV (S_2, green), respectively, due to the holes in previously occupied n and π orbitals, respectively, for the valence-excited states − in full analogy with the O 1s PP-NEXAFS spectra.

Analyzing the time-resolved N K-edge difference spectrum TR-NEXAFS in Figure 7b, we first note two positive absorption bands (red areas) near 399 and 406 eV. The lower-energy band at 399 eV shows a gradual decrease in intensity over the first ∼150 fs, accompanied by a small blue-shift (by less than 1 eV). The most prominent low-energy ground state bleach (blue) is found near 403 eV, where the GS NEXAFS spectrum showed a shoulder (the lowest-energy peak "A" in ref 69). In the stationary S_1 PP-NEXAFS spectrum, a distinct feature was also observed at 402 eV; however, no corresponding signal is present in the TR-NEXAFS spectrum, despite one might expect such a feature emerging when a $S_2 \rightarrow$

https://doi.org/10.1021/acsomega.6c06959
ACS Omega 2026, 11, 56251−56264

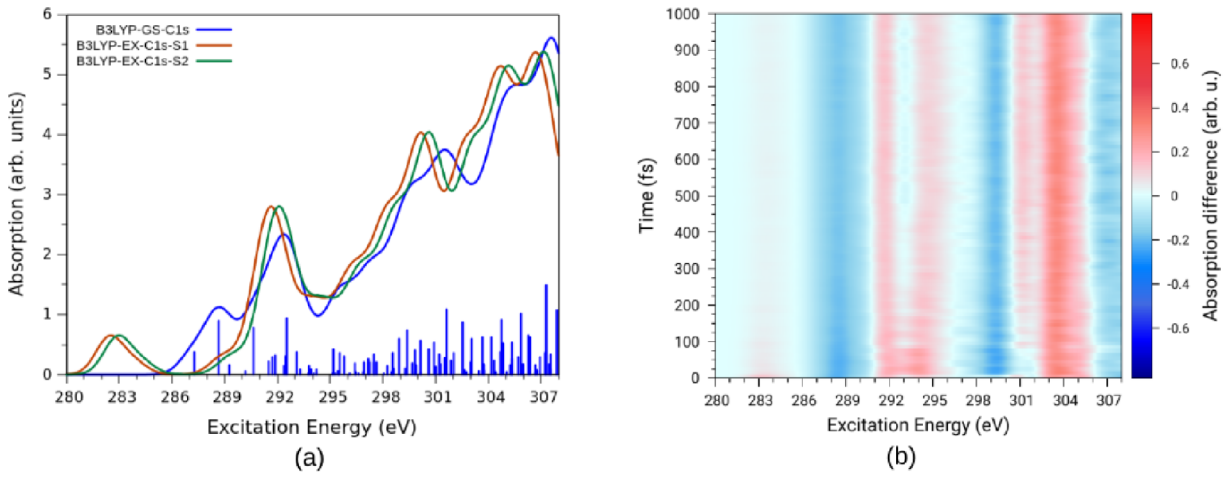


Figure 8. (a) Broadened C 1s GS-NEXAFS spectrum (with underlying stick spectrum) and PP-NEXAFS spectra for the S_1 and S_2 states of uracil. (b) Time-resolved C 1s NEXAFS spectrum (TR-NEXAFS) following photoexcitation.

S_1 transition took place. Apparently, the lack of such a feature (associated with S_1) in the TR-NEXAFS spectrum is caused by a dynamical effect. In addition to the spectral intensity in the low-energy region, a new absorption feature emerges near 410 eV at later times, around 100 fs. At similar time a positive features disappears around 416 eV. Such behavior could be associated with changes in electronic character or molecular geometry during excited-state relaxation.

The atom-resolved N 1s TR-NEXAFS spectra were computed (Figure 6c,d). For N2-resolved spectra, a main absorption feature near 399 eV gradually decreases in intensity after approximately 100 fs, consistent with population transfer from S_2 to S_1 seen in TSH simulations. The average N2−C3 and N2−C4 bond lengths do not exhibit substantial net change over time (see Figure 3e,f), short-time oscillations are observed within the first ∼150 fs. Concurrently the absorption feature near 407 eV demonstrates some oscillations, and remains relatively static in both energy and intensity after ∼150 fs. The 410 eV positive feature, which was seen in case of overall N 1s TR-NEXAFS spectrum (Figure 7), is absent in the N2-resolved spectrum (Figure 6c). This indicates that the appearance of 410 eV feature is not associated with N2.

In contrast, N1, the N atom sandwiched between the two C═O groups, exhibits more pronounced temporal changes. The higher-energy absorption band, initially spanning 414−417 eV, gradually decreases in intensity. Subsequently, a new feature at approximately 410 eV appears within the first ∼150 fs. Meanwhile, the lower-energy feature near 398 eV shows a very slight blue-shift toward 400 eV. The spectral appearance at ∼410 eV is attributed to internal conversion from the bright S_2 to the dark S_1 state, accompanied by nuclear motions localized around the N1 site. These spectral features likely arise from orbital reorganization and reduced oscillator strength linked to local bonding changes, such as the shortening of the N1−C6 bond and elongation of N1−C3 (see Figure 3c,d).

Overall, also the N 1s NEXAFS spectra reflect the $S_2 \rightarrow S_1$ nonadiabatic transition on a ∼140 fs time scale, after which only weak residual spectral features coming from S_1 remain, showing that internal conversion to the ground state (S_0) occurs on a longer time scale than covered in the present simulations. Further, a clear asymmetry between the N atoms is seen, similar to the one for the two O atoms, highlighting the sensitivity of TR-NEXAFS to both local bond reorganization and nonlocal electronic effects.

3.2.3. C 1s Stationary and TR-NEXAFS Spectra. Finally, the C 1s NEXAFS spectra of uracil were studied. The static GS-NEXAFS and S_1, S_2−PP-NEXAFS C 1s spectra are presented in Figure 8a. For the C 1s GS-NEXAFS spectrum, absorption starts at ∼287 eV with continuous increase in intensity until 307 eV. Closer inspection shows that under the low-energy peak centered around 288 eV, four dominating peaks are found, corresponding to excitations from the four C 1s orbitals into the LUMO, at 287.3 eV (for C5), 288.6 eV (for C4), 290.7 eV (C6), and 292.5 eV (C3). The experimental C 1s NEXAFS spectrum of uracil finds four well-resolved lowest-energy peaks "A" to "D" in ref 69, at 284.8, 286.1, 288.0, and 289.5 eV, respectively. According to ADC(2)/6-31+G calculations, these peaks are dominated by the C 1s → π^* (LUMO) transitions, located (after an empirical −2.46 eV shift), at 284.4 eV (C5), 286.1 eV (C4), 288.0 eV (C6), and 289.5 eV (C3), respectively. That is, w.r.t. experiment we have a blue-shift again (of ∼2−3 eV), while the peak splittings are very good in this case. ADC2 gives similar results[69] when no shift is made, and the assignment of dominant peaks contributing to A-D is the same as here.

Concerning the PP-NEXAFS spectra, we see from Figure 8a for both S_1 and S_2 new absorption features at 282−284 eV. Again, the additional signals reflect transitions into the hole orbitals created by the initial excitation, where the S_1 peak at 282 eV is due to the hole generated in the n-orbital and the S_2 peak at 283 eV due to the hole in the π-orbital. Further, the ground state signal around 288 eV, has clearly lost intensity in the PP-NEXAFS spectra, which would probably contribute to a ground state bleach in the C 1s TR-NEXAFS spectra. Finally, at the higher-energy region around 298−305 eV, S_1 and S_2 peaks are shifted slightly relative to GS, which may manifest in TR-NEXAFS spectra as well.

The carbon K-edge TR-NEXAFS difference spectrum (Figure 8b) consists of three main positive absorption bands centered near 283, 293, and 304 eV, each showing distinct temporal evolution. The lowest-energy ground state bleach (blue areas) is observed near 288 eV, as expected. The earliest spectral feature at 283 eV, undergoes a rapid decay within the first 15−20 fs. This transient signal loss is attributed to immediate structural deformation in the S_2 excited-state,

https://doi.org/10.1021/acsomega.6c06959
ACS Omega 2026, 11, 56251−56264

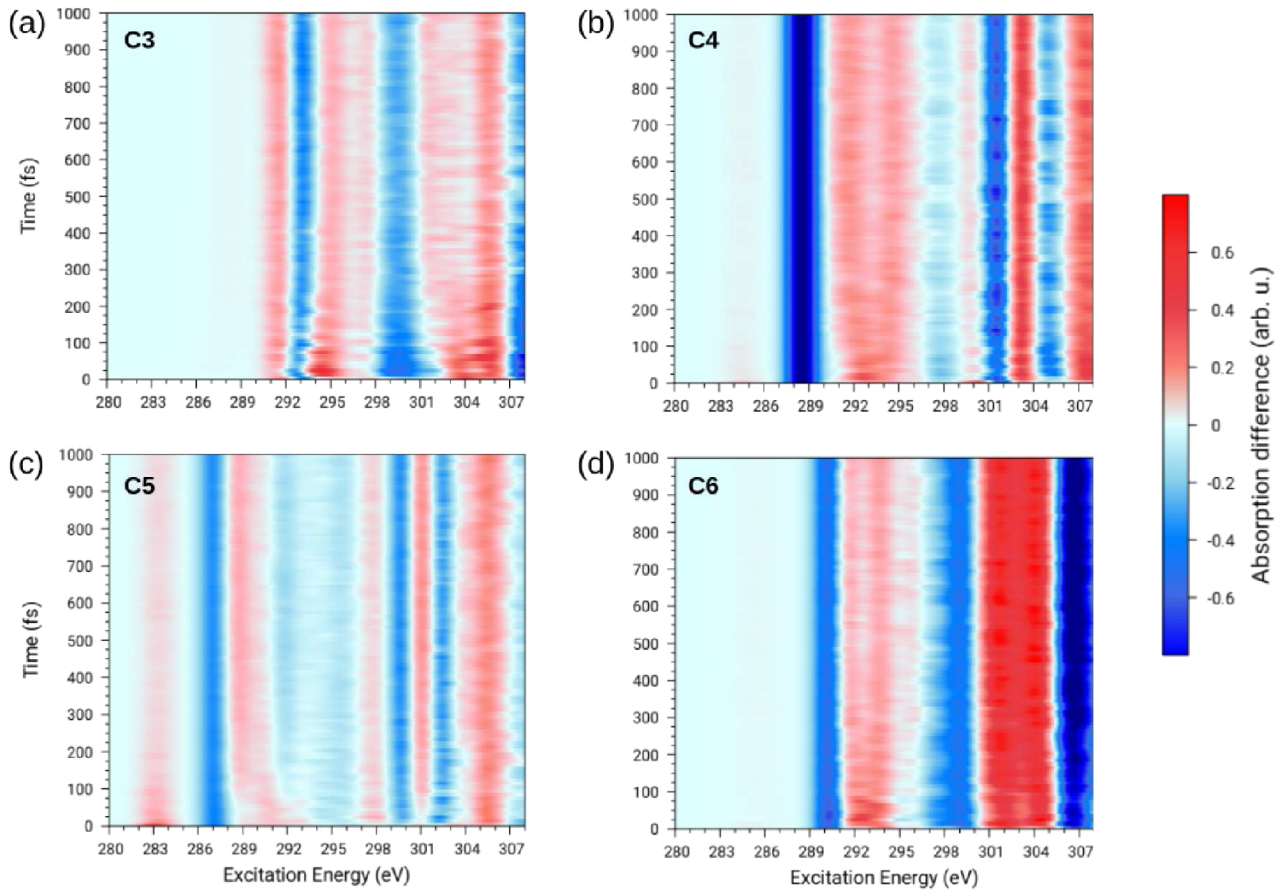


Figure 9. Atom-resolved TR-NEXAFS of the uracil molecule. (a), (b), (c) and (d) represent the C3, C4, C5 and C6 atom-resolved TR-NEXAFS of uracil, respectively. See Figure 1b for atom numbering.

particularly involving C−C double bond elongation and initial out-of-plane distortions of the pyrimidine ring after photoexcitation. Our surface hopping simulations confirm that strong out-of-plane distortions (strong change in dihedral angles) and bond-length modulations (see Figure 3g−i and Figure 4g−i) occur within this timeframe, especially at C4−C5 and adjacent atoms, disrupting π-conjugation and thereby altering the character of high-lying occupied orbitals (participating in hole-refilling). These geometric perturbations presumably reduce the overlap of core to valence transitions that initially (*i.e.*, after initial excitation mainly into S_2), contribute to the 283 eV band, leading to its ultrafast disappearance.

The second decaying, positive feature of interest, centered at 293 eV, decreases more slowly and is largely suppressed by around 100 fs. This evolution coincides with the internal conversion from the bright S_2 ($\pi\pi^*$) state to the dark S_1 ($n\pi^*$) state, as revealed by the surface hopping population dynamics (Figure 2). Concurrently, a new absorption feature emerges around 301 eV, marking a distinct spectral signature of S_1 population. Although both states (S_1 and S_2) have comparable static intensities at this energy, the dynamic buildup of this feature correlates with the rise of S_1 population, suggesting that structural and electronic relaxation in the $n\pi^*$ state enhances the relevant core to valence transitions. In particular, reorganization of the low-lying unoccupied orbitals influenced by lone-pair participation on heteroatoms and altered π-conjugation modifies their energy levels and spatial overlap with carbon 1s orbitals, thereby enabling transitions not prominent at earlier times. The spectral contrast between the 293 eV decay and the 301 eV rise is consistent with electronic state conversion. We also note that the C 1s TR-NEXAFS spectral features were found to be preserved across different ensemble sizes, as shown by comparisons using 20 and 40 trajectories (see Supporting Information, Figure S1).

In addition to electronic effects, the C 1s TR-NEXAFS spectra reveal a strong sensitivity to site-specific structural reorganization. The carbon atoms most directly involved in the early-time spectral shifts, C4 and C5, undergo significant angle displacement and bond rehybridization according to the TSH data (see Figure 3g−i and Figure 4g−i). This is also reflected in the *atom-resolved* TR-NEXAFS spectra, shown in Figure 9, according to which the early-time spectral shifts are mainly observed for C4 and C5.

In general, compared to O 1s and N 1s atom-resolved TR-NEXAFS, the atom-resolved C 1s TR-NEXAFS spectra are more diffuse and have more positive−negative absorption pairs. Due to its substantial spectral overlap, it is relatively difficult to assign unique site-specific signatures. Still, a few characteristic features can be observed from the C 1s atom-resolved spectrum. At lower photon energies (~283 eV), the most prominent transient signal originates from the C5 site, which shows a strong positive feature that diminishes as the delay time increases. At the same energy, the C4 site also exhibits a weak positive contribution at ~284 eV. These low-energy features are closely correlated with the structural dynamics of the C4−C5 double bond, as revealed by the bond

https://doi.org/10.1021/acsomega.6c06959
ACS Omega 2026, 11, 56251−56264

length and bond angle changes observed in the SH simulations (see Figure 3g–i).

Strong ground-state bleach signals are observed for both C4 and C5. For C4, the bleach is centered at 289 eV, whereas for C5 it appears at slightly lower energies (~287–288 eV). The C6 site also displays a pronounced bleach at 290–291 eV, along with a higher-energy bleach at 307 eV. In addition, C6 exhibits a broad and intense positive absorption band between 301 and 304 eV. The temporal evolution of the C5 spectrum reveals a notable spectral shift within the first 100–120 fs. Initially, a positive feature is observed at 293 eV, which gradually redshifts to ~290 eV. Concurrently, the C5 feature at ~301 eV increases in intensity. This coupled redshift and growth behavior is consistent with internal conversion dynamics occurring during this early-time window. In the same region (around 302 eV) the C3 spectrum also has some contributions: the negative features redshifts to 301 eV and the positive feature from 304 eV redshifts toward 301 eV.

4. SUMMARY AND CONCLUSIONS

In this paper, we presented an investigation of the early $S_2 \rightarrow S_1$ relaxation dynamics of uracil using a combination of surface hopping and TR-NEXAFS simulations at the O 1s, N 1s, and C 1s edges. The simulations do not capture the subsequent recovery to the ground state within the simulated time window. For the $S_2 \rightarrow S_1$ dynamics, we characterized the interplay between electronic relaxation and nuclear motion following UV photoexcitation, and established site-specific signatures of these processes through core-level spectroscopy.

Surface hopping dynamics initiated in the bright S_2 ($\pi\pi^*$) state revealed a rapid and efficient internal conversion to the dark S_1 ($n\pi^*$) state within the first ~140 fs. No trajectories returned to the ground state (S_0), which may be partially attributed to the nature of the underlying TD-DFT methodology. Nevertheless, the simulations captured the key aspects of excited-state dynamics, particularly the population trapping in S_1 and the accompanying nuclear distortions. Detailed structural analyses revealed localized changes near the oxygen, nitrogen and ethylenic carbon centers, including shortening and lengthening of the carbonyl bond and asynchronous motion at the N1 and N2 sites as well as ring puckering associated with the C4–C5 bond.

Building on these dynamic structural results, we coupled our TR-NEXAFS simulations with the TSH calculations to capture how the local chemical environments evolve in real time across multiple atomic sites. At the oxygen edge, a pronounced asymmetry was observed between O7 and O8: O7 exhibited both a strong stationary peak at 529 eV and a dynamic, blue-shifting band (535 to 537 eV) correlated with C6–O7 bond elongation. In contrast, O8 showed minimal evolution, reflecting its limited role in the excited-state reorganization.

Nitrogen-resolved TR-NEXAFS revealed more diffuse features, indicative of overlapping state contributions. N2 showed gradual intensity decay at 399 eV, tracking S_2 population loss, while N1 exhibited a pronounced change: the 414–417 eV absorption band diminished and a new feature emerged at ~410 eV, indicating internal conversion ($S_2 \rightarrow S_1$) at around 140 fs. These findings highlight the distinct and asynchronous involvement of the two nitrogen atoms during relaxation.

Finally, the carbon K-edge TR-NEXAFS spectrum shows rapid π-conjugation loss from torsional deformation of the pyrimidine ring resulted from C4 and C5 carbons within 25 fs at 282 eV. The 293 eV feature gradually weakens and simultaneously a new absorption feature emerges near 301 eV indicating internal conversion (~140 fs) from the delocalized S_2 ($\pi\pi^*$) to the more localized S_1 ($n\pi^*$) state.

In summary, our TSH dynamics leave clear traces in the TR-NEXAFS spectra. In concert, TR-NEXAFS and nonadiabatic molecular dynamics give us a clear picture of coupled electron-nuclear dynamics after photoexcitation, enabling direct comparison with gas-phase TR-NEXAFS experiments in the future. In this work, for uracil, the combined approach reveals not only the key relaxation pathways but also the atomic sites most affected by photoinduced reorganization, offering an atom- and time-resolved understanding of ultrafast processes relevant to nucleobase photophysics. Inclusion of triplet states in TSH simulations in the context of TR-NEXAFS calculations should be addressed in the future research.

■ ASSOCIATED CONTENT

Data Availability Statement

Data for this article are available at Zenodo at 10.5281/zenodo.19735475.

Supporting Information

The Supporting Information is available free of charge at https://pubs.acs.org/doi/10.1021/acsomega.6c06959.

Further results for C 1s TR-NEXAFS (PDF)

■ AUTHOR INFORMATION

Corresponding Author

Peter Saalfrank − *University of Potsdam, Institute of Chemistry, Theoretical Chemistry, Potsdam 14476, Germany*; orcid.org/0000-0002-5988-5945; Email: peter.saalfrank@uni-potsdam.de

Authors

Bonasree Roy − *University of Potsdam, Institute of Chemistry, Theoretical Chemistry, Potsdam 14476, Germany*; orcid.org/0009-0004-6232-2889

Evgenii Titov − *University of Potsdam, Institute of Chemistry, Theoretical Chemistry, Potsdam 14476, Germany*; orcid.org/0000-0002-1732-1826

Complete contact information is available at: https://pubs.acs.org/10.1021/acsomega.6c06959

Notes

The authors declare no competing financial interest.

■ ACKNOWLEDGMENTS

We thank Nicolas Jahn (Potsdam) for technical support and discussions. We also thank Markus Gühr and Julius Schwarz (both from Hamburg) for fruitful discussions. Financial support by the Deutsche Forschungsgemeinschaft (DFG, German Research Foundation) via CRC/SFB 1636 − Project ID 510943930 − Project Nos. A03 and B05 is gratefully acknowledged.

■ REFERENCES

(1) Improta, R.; Santoro, F.; Blancafort, L. Quantum mechanical studies on the photophysics and the photochemistry of nucleic acids and nucleobases. *Chem. Rev.* **2016**, *116* (6), 3540–3593.

(2) Gustavsson, T.; Improta, R.; Markovitsi, D. DNA/RNA: building blocks of life under UV irradiation. *J. Phys. Chem. Lett.* **2010**, *1* (13), 2025−2030.
(3) Crespo-Hernández, C. E.; Cohen, B.; Hare, P. M.; Kohler, B. Ultrafast excited-state dynamics in nucleic acids. *Chem. Rev.* **2004**, *104* (4), 1977−2020.
(4) Jochims, H.-W.; Schwell, M.; Baumgärtel, H.; Leach, S. Photoion mass spectrometry of adenine, thymine and uracil in the 6−22 eV photon energy range. *Chem. Phys.* **2005**, *314* (1), 263−282.
(5) Robinson, M. S.; Niebuhr, M.; Gühr, M. Ultrafast photo-ion probing of the relaxation dynamics in 2-thiouracil. *Molecules* **2023**, *28* (5), 2354.
(6) Roy, B.; Titov, E.; Robinson, M. S.; Gühr, M.; Saalfrank, P. Dissociative photoionization of 2-thiouracil and 4-thiouracil: A molecular dynamics study. *J. Phys. Chem. A* **2025**, *129* (32), 7352−7364.
(7) Middleton, C. T.; De La Harpe, K.; Su, C.; Law, Y. K.; Crespo-Hernández, C. E.; Kohler, B. DNA excited-state dynamics: From single bases to the double helix. *Annu. Rev. Phys. Chem.* **2009**, *60*, 217−239.
(8) Keefer, D.; Thallmair, S.; Matsika, S.; de Vivie-Riedle, R. Controlling photorelaxation in uracil with shaped laser pulses: A theoretical assessment. *J. Am. Chem. Soc.* **2017**, *139* (14), 5061−5066.
(9) Richter, M.; Mai, S.; Marquetand, P.; González, L. Ultrafast intersystem crossing dynamics in uracil unravelled by ab initio molecular dynamics. *Phys. Chem. Chem. Phys.* **2014**, *16* (44), 24423−24436.
(10) Faccialã, D.; Bonanomi, M.; Tenorio, B. N. C.; Avaldi, L.; Bolognesi, P.; Callegari, C.; Coreno, M.; Coriani, S.; Decleva, P.; Devetta, M.; Došlić, N.; De Fanis, A.; Di Fraia, M.; Lever, F.; Mazza, T.; Meyer, M.; Mullins, T.; Ovcharenko, Y.; Pal, N.; Piancastelli, M. N.; Richter, R.; Rivas, D. E.; Sapunar, M.; Senfftleben, B.; Usenko, S.; Vozzi, C.; Gühr, M.; Prince, K. C.; Plekan, O. Unraveling the relaxation dynamics of uracil: Insights from time-resolved X-ray photoelectron spectroscopy. *J. Am. Chem. Soc.* **2025**, *147* (34), 30694−30707.
(11) Park, W.; Filatov, M.; Sadiq, S.; Gerasimov, I.; Lee, S.; Joo, T.; Choi, C. H. A plausible mechanism of uracil photohydration involves an unusual intermediate. *J. Phys. Chem. Lett.* **2022**, *13* (30), 7072−7080.
(12) Chakraborty, P.; Liu, Y.; Weinacht, T.; Matsika, S. Effect of dynamic correlation on the ultrafast relaxation of uracil in the gas phase. *Faraday Discuss.* **2021**, *228*, 266−285.
(13) Nachtigallová, D.; Aquino, A. J. A.; Szymczak, J. J.; Barbatti, M.; Hobza, P.; Lischka, H. Nonadiabatic dynamics of uracil: Population split among different decay mechanisms. *J. Phys. Chem. A* **2011**, *115*, 5247−5255.
(14) Matsika, S.; Spanner, M.; Kotur, M.; Weinacht, T. C. Ultrafast relaxation dynamics of uracil probed via strong field dissociative ionization. *J. Phys. Chem. A* **2013**, *117* (48), 12796−12801.
(15) Matsika, S. Radiationless decay of excited states of uracil through conical intersections. *J. Phys. Chem. A* **2004**, *108* (37), 7584−7590.
(16) Zgierski, M. Z.; Patchkovskii, S.; Fujiwara, T.; Lim, E. C. On the origin of the ultrafast internal conversion of electronically excited pyrimidine bases. *J. Phys. Chem. A* **2005**, *109* (42), 9384−9387.
(17) Merchan, M.; Gonzalez-Luque, R.; Climent, T.; Serrano-Andres, L.; Rodríguez, E.; Reguero, M.; Pelaez, D. Unified model for the ultrafast decay of pyrimidine nucleobases. *J. Phys. Chem. B* **2006**, *110* (51), 26471−26476.
(18) Hudock, H. R.; Levine, B. G.; Thompson, A. L.; Satzger, H.; Townsend, D.; Gador, N.; Ullrich, S.; Stolow, A.; Martinez, T. J. Ab initio molecular dynamics and time-resolved photoelectron spectroscopy of electronically excited uracil and thymine. *J. Phys. Chem. A* **2007**, *111* (34), 8500−8508.
(19) Mercier, Y.; Santoro, F.; Reguero, M.; Improta, R. The decay from the dark $n\pi^*$ excited state in uracil: An integrated CASPT2/CASSCF and PCM/TD-DFT study in the gas phase and in water. *J. Phys. Chem. B* **2008**, *112* (35), 10769−10772.
(20) Bäuml, L.; Rott, F.; Schnappinger, T.; de Vivie-Riedle, R. Following the nonadiabatic ultrafast dynamics of uracil via simulated X-ray absorption spectra. *J. Phys. Chem. A* **2023**, *127* (46), 9787−9796.
(21) Ghafur, O.; Crane, S. W.; Ryszka, M.; Bockova, J.; Rebelo, A.; Saalbach, L.; De Camillis, S.; Greenwood, J. B.; Eden, S.; Townsend, D. Ultraviolet relaxation dynamics in uracil: Time-resolved photoion yield studies using a laser-based thermal desorption source. *J. Chem. Phys.* **2018**, *149* (3), 034301.
(22) Canuel, C.; Mons, M.; Piuzzi, F.; Tardivel, B.; Dimicoli, I.; Elhanine, M. Excited states dynamics of DNA and RNA bases: Characterization of a stepwise deactivation pathway in the gas phase. *J. Chem. Phys.* **2005**, *122* (7), 074316.
(23) Kang, H.; Lee, K. T.; Jung, B.; Ko, Y. J.; Kim, S. K. Intrinsic lifetimes of the excited state of DNA and RNA bases. *J. Am. Chem. Soc.* **2002**, *124* (44), 12958−12959.
(24) Ullrich, S.; Schultz, T.; Zgierski, M. Z.; Stolow, A. Electronic relaxation dynamics in DNA and RNA bases studied by time-resolved photoelectron spectroscopy. *Phys. Chem. Chem. Phys.* **2004**, *6* (10), 2796−2801.
(25) He, Y.; Wu, C.; Kong, W. Decay pathways of thymine and methyl-substituted uracil and thymine in the gas phase. *J. Phys. Chem. A* **2003**, *107* (26), 5145−5148.
(26) Perun, S.; Sobolewski, A. L.; Domcke, W. Conical intersections in thymine. *J. Phys. Chem. A* **2006**, *110* (49), 13238−13244.
(27) Hentschel, M.; Kienberger, R.; Spielmann, C.; Reider, G. A.; Milosevic, N.; Brabec, T.; Corkum, P.; Heinzmann, U.; Drescher, M.; Krausz, F. Attosecond metrology. *Nature* **2001**, *414* (6863), 509−513.
(28) Krausz, F.; Ivanov, M. Attosecond physics. *Rev. Mod. Phys.* **2009**, *81* (1), 163−234.
(29) Zewail, A. H. Femtochemistry: Atomic-scale dynamics of the chemical bond. *J. Phys. Chem. A* **2000**, *104* (24), 5660−5694.
(30) Nisoli, M.; Decleva, P.; Calegari, F.; Palacios, A.; Martín, F. Attosecond electron dynamics in molecules. *Chem. Rev.* **2017**, *117* (16), 10760−10825.
(31) Mukamel, S. Multidimensional femtosecond correlation spectroscopies of electronic and vibrational excitations. *Annu. Rev. Phys. Chem.* **2000**, *51* (1), 691−729.
(32) Schnappinger, T.; Jadoun, D.; Gudem, M.; Kowalewski, M. Time-resolved X-ray and XUV based spectroscopic methods for nonadiabatic processes in photochemistry. *Chem. Commun.* **2022**, *58* (92), 12763−12781.
(33) List, N. H.; Dempwolff, A. L.; Dreuw, A.; Norman, P.; Martínez, T. J. Probing competing relaxation pathways in malonaldehyde with transient X-ray absorption spectroscopy. *Chem. Sci.* **2020**, *11* (16), 4180−4193.
(34) Scutelnic, V.; Tsuru, S.; Pápai, M.; Yang, Z.; Epshtein, M.; Xue, T.; Haugen, E.; Kobayashi, Y.; Krylov, A. I.; Møller, K. B.; et al. X-ray transient absorption reveals the $1A_u$ ($n\pi^*$) state of pyrazine in electronic relaxation. *Nat. Commun.* **2021**, *12* (1), 5003.
(35) Datar, A.; Gudivada, S.; Matthews, D. A. Ab initio investigation of intramolecular charge transfer states in dmabn by calculation of excited state x-ray absorption spectra. *J. Phys. Chem. A* **2023**, *127* (21), 4643−4649.
(36) Neville, S. P.; Chergui, M.; Stolow, A.; Schuurman, M. S. Ultrafast X-ray spectroscopy of conical intersections. *Phys. Rev. Lett.* **2018**, *120* (24), 243001.
(37) Tsuru, S.; Vidal, M. L.; Pápai, M.; Krylov, A. I.; Møller, K. B.; Coriani, S. Time-resolved near-edge X-ray absorption fine structure of pyrazine from electronic structure and nuclear wave packet dynamics simulations. *J. Chem. Phys.* **2019**, *151* (12), 124114.
(38) Wachulak, P.; Duda, M.; Bartnik, A.; Węgrzyński, Ł.; Fok, T.; Fiedorowicz, H. NEXAFS at nitrogen K-edge and titanium L-edge using a laser-plasma soft X-ray source based on a double-stream gas puff target. *APL Photonics* **2019**, *4* (3), 030807.
(39) Ehlert, C.; Gühr, M.; Saalfrank, P. An efficient first principles method for molecular pump-probe NEXAFS spectra: Application to thymine and azobenzene. *J. Chem. Phys.* **2018**, *149* (14), 144112.

https://doi.org/10.1021/acsomega.6c06959
ACS Omega 2026, 11, 56251−56264

(40) Ehlert, C.; Klamroth, T. Psixas: A psi4 plugin for efficient simulations of X-ray absorption spectra based on the transition-potential and δ-kohn−sham method. *J. Comput. Chem.* **2020**, *41* (19), 1781−1789.
(41) Becke, A. D. Density-functional thermochemistry. III. The role of exact exchange. *J. Chem. Phys.* **1993**, *98*, 5648−5652.
(42) Stephens, P. J.; Devlin, F. J.; Chabalowski, C. F.; Frisch, M. J. Ab initio calculation of vibrational absorption and circular dichroism spectra using density functional force fields. *J. Phys. Chem.* **1994**, *98*, 11623−11627.
(43) Weigend, F.; Ahlrichs, R. Balanced basis sets of split valence, triple zeta valence and quadruple zeta valence quality for H to Rn: Design and assessment of accuracy. *Phys. Chem. Chem. Phys.* **2005**, *7*, 3297−3305.
(44) Grimme, S.; Antony, J.; Ehrlich, S.; Krieg, H. A consistent and accurate ab initio parametrization of density functional dispersion correction (DFT-D) for the 94 elements h-pu. *J. Chem. Phys.* **2010**, *132* (15), 154104.
(45) Grimme, S.; Ehrlich, S.; Goerigk, L. Effect of the damping function in dispersion corrected density functional theory. *J. Comput. Chem.* **2011**, *32* (7), 1456−1465.
(46) Neese, F. Software update: The ORCA program system—Version 5.0. *WIREs Comput. Mol. Sci.* **2022**, *12* (5), No. e1606.
(47) Wigner, E. On the quantum correction for thermodynamic equilibrium. *Phys. Rev.* **1932**, *40*, 749−759.
(48) Mai, S.; Avagliano, D.; Heindl, M.; Marquetand, P.; Menger, M. F. S. J.; Oppel, M.; Plasser, F.; Polonius, S.; Ruckenbauer, M.; Shu, Y., et al. *SHARC3.0: Surface hopping including arbitrary couplings—program package for non-adiabatic dynamics*; Zenodo, 2023.
(49) Mai, S.; Marquetand, P.; González, L. Nonadiabatic dynamics: The SHARC approach. *WIREs Comput. Mol. Sci.* **2018**, *8* (6), No. e1370.
(50) Tully, J. C. Molecular dynamics with electronic transitions. *J. Chem. Phys.* **1990**, *93*, 1061−1071.
(51) Verlet, L. Computer "experiments" on classical fluids. I. Thermodynamical properties of Lennard-Jones molecules. *Phys. Rev.* **1967**, *159*, 98.
(52) Granucci, G.; Persico, M.; Toniolo, A. Direct semiclassical simulation of photochemical processes with semiempirical wave functions. *J. Chem. Phys.* **2001**, *114*, 10608−10615.
(53) Plasser, F.; Ruckenbauer, M.; Mai, S.; Oppel, M.; Marquetand, P.; González, L. Efficient and flexible computation of many-electron wave function overlaps. *J. Chem. Theory Comput.* **2016**, *12*, 1207−1219.
(54) Granucci, G.; Persico, M. Critical appraisal of the fewest switches algorithm for surface hopping. *J. Chem. Phys.* **2007**, *126* (13), 134114.
(55) Granucci, G.; Persico, M.; Zoccante, A. Including quantum decoherence in surface hopping. *J. Chem. Phys.* **2010**, *133* (13), 134111.
(56) Ehlert, C.; Holzweber, M.; Lippitz, A.; Unger, W. E. S.; Saalfrank, P. A detailed assignment of NEXAFS resonances of imidazolium based ionic liquids. *Phys. Chem. Chem. Phys.* **2016**, *18*, 8654−8661.
(57) Smith, D. G. A.; Burns, L. A.; Simmonett, A. C.; Parrish, R. M.; Schieber, M. C.; Galvelis, R.; Kraus, P.; Kruse, H.; Di Remigio, R.; Alenaizan, A.; et al. Psi4 1.4: Open-source software for high-throughput quantum chemistry. *J. Chem. Phys.* **2020**, *152* (18), 184108.
(58) Jahn, N.; Titov, E.; Saalfrank, P. Ground state quantum chemistry, excited state dynamics, and time-resolved x-ray absorption spectroscopy of substituted thiophenols. *J. Chem. Phys.* **2025**, *163* (17), 174304.
(59) Neiss, C.; Saalfrank, P.; Parac, M.; Grimme, S. Quantum chemical calculation of excited states of flavin-related molecules. *J. Phys. Chem. A* **2003**, *107* (1), 140−147.
(60) Clark, L. B.; Peschel, G. G.; Tinoco, I. Vapor spectra and heats of vaporization of some purine and pyrimidine bases. *J. Phys. Chem.* **1965**, *69*, 3615−3618.
(61) Martin, R. L. Natural transition orbitals. *J. Chem. Phys.* **2003**, *118*, 4775−4777.
(62) Fedotov, D. A.; Paul, A. C.; Posocco, P.; Santoro, F.; Garavelli, M.; Koch, H.; Coriani, S.; Improta, R. Excited-state absorption of uracil in the gas phase: Mapping the main decay paths by different electronic structure methods. *J. Chem. Theory Comput.* **2021**, *17*, 1638−1652.
(63) Improta, R.; Barone, V. Absorption and fluorescence spectra of uracil in the gas phase and in aqueous solution: A TD-DFT quantum mechanical study. *J. Am. Chem. Soc.* **2004**, *126*, 14320−14321.
(64) Lan, Z.; Fabiano, E.; Thiel, W. Photoinduced nonadiabatic dynamics of pyrimidine nucleobases: On-the-fly surface-hopping study with semiempirical methods. *J. Phys. Chem. B* **2009**, *113*, 3548−3555.
(65) Kong, W.; He, Y.; Wu, C. Decay pathways of pyrimidine bases: From gas phase to solution. In *Radiation Induced Molecular Phenomena in Nucleic Acids: a Comprehensive Theoretical and Experimental Analysis*; Springer, 2008; pp. 301−321.
(66) Miura, Y.; Yamamoto, Y.-I.; Karashima, S.; Orimo, N.; Hara, A.; Fukuoka, K.; Ishiyama, T.; Suzuki, T. Formation of long-lived dark states during electronic relaxation of pyrimidine nucleobases studied using extreme ultraviolet time-resolved photoelectron spectroscopy. *J. Am. Chem. Soc.* **2023**, *145* (6), 3369−3381.
(67) Milovanović, B.; Novak, J.; Etinski, M.; Domcke, W.; Došlić, N. Simulation of uv absorption spectra and relaxation dynamics of uracil and uracil−water clusters. *Phys. Chem. Chem. Phys.* **2021**, *23*, 2594−2604.
(68) Chakraborty, P.; Liu, Y.; McClung, S.; Weinacht, T.; Matsika, S. Time resolved photoelectron spectroscopy as a test of electronic structure and nonadiabatic dynamics. *J. Phys. Chem. Lett.* **2021**, *12* (21), 5099−5104.
(69) Feyer, V.; Plekan, O.; Richter, R.; Coreno, M.; de Simone, M.; Prince, K. C.; Trofimov, A. B.; Zaytseva, I. L.; Schirmer, J. Tautomerism in cytosine and uracil: A theoretical and experimental X-ray absorption and resonant Auger study. *J. Phys. Chem. A* **2010**, *114* (37), 10270−10276.

https://doi.org/10.1021/acsomega.6c06959
ACS Omega 2026, 11, 56251−56264